Seismicity and self-organized criticality

B. Barriere and D. L. Turcotte
Department of Geological Sciences, Cornell University, Ithaca, New York 14850
(Received 16 July 1993)

Distributed seismicity appears to fit the definition of a self-organized, critical phenomenon. In this paper a cellular-automata model is presented as an analog to distributed seismicity. We consider a grid of boxes with a fractal distribution of sizes. Particles are randomly added to the boxes. When the number of particles reaches a critical value they are redistributed to adjacent boxes and edge or corner boxes lose particles off the grid. The addition of particles is analogous to crustal strain and the redistribution from a box is equivalent to a characteristic earthquake on a fault. A redistribution from a small box (a foreshock) may trigger an instability in a larger box (the main shock). A redistribution from a large box always triggers many instabilities in adjacent smaller boxes (aftershocks). The frequency-size statistics for both main shocks and aftershocks satisfy the Gutenberg-Richter relation. Model foreshocks occur 28% of the time, in good agreement with actual foreshocks. No systematic precursors are observed prior to model earthquakes, also in agreement with the present status of earthquake prediction studies.

PACS number(s): 05.40.+j, 05.45.+b

I. INTRODUCTION

The concept of self-organized criticality [1] is defined to be a natural system in a marginally stable state, evolving naturally back to the state of marginal stability when perturbed from that state. The input to the system is continuous but the loss is in a discrete set of events that satisfy fractal frequency-size statistics.

In the original cellular-automata model for self-organized criticality a two-dimensional grid of boxes was considered. Particles were added randomly to the boxes until there were four particles in a box. The box was then considered unstable and the four particles were redistributed to the four adjacent boxes. If any of those boxes had four or more particles, a further redistribution of elements was carried out. Particles were lost only from the sides of the grid. A fractal (power-law) relation was found [2] between the number of events and the number of particles lost in each event. These events were said to be analogous to sandslides on sandpiles due to the random addition of sand grains. A number of groups have studied actual sandpiles and in some cases fractal distributions of sandslides have been found [3].

Although there are important similarities between distributed seismicity and simple cellular automata models [4], there are also significant differences. There are no recognized foreshocks or aftershocks. A particular element can participate in both small and large events, and particular elements are not associated with characteristic earthquakes. They also lack much of the basic physics such as stick-slip behavior and elastic rebound. A simple model that includes both consists of two sliding blocks coupled to each other and to a constant velocity driver by springs [5]. It has been shown that any asymmetry in this model results in classical chaotic behavior; the Feigenbaum period-doubling route to chaos is observed [6].

A model that combines the analog features of slider blocks and the high-order aspects of cellular-automata models involves the use of many slider blocks. For linear arrays of up to 400 blocks, slip events involving large numbers of blocks were observed, the motion of all blocks involved in a slip event were coupled, and the applicable equations of motion had to be solved simultaneously [7]. Although the system is completely deterministic, the behavior was apparently chaotic. Frequency-size statistics were obtained for slip events and the events fell into two groups: smaller events obeyed a power-law (fractal) relationship and an anomalously large number of large events included all the slider blocks. This model was considered to be a model for the behavior of a single fault, not a model for distributed seismicity. The large events were associated with characteristic earthquakes on the fault and smaller events with background seismicity on the fault between characteristic earthquakes.

An alternative model combined features of the cellular-automata model and the slider-block model [8]. A linear array of slider blocks was considered but only one block was allowed to slip in a given time step. The slip of one block could lead to the instability of either or both of the adjacent blocks, which would then be allowed to slip in a subsequent step or steps until all blocks were again stable. A variety of related models have been proposed [9].

In order to better understand earthquakes, it is essential to determine whether concepts of self-organized criticality are applicable. Scholz [10] argues that the earth's upper crust is everywhere in a state of self-organized criticality. He cites as evidence the occurrence of earthquakes in the interiors of the surface plates as well as at the boundaries, although the level of seismicity is much lower in the interiors. An example of these interior earthquakes was the sequence of three very large earthquakes ($m \approx 8$) that occurred near New Madrid, Missouri, in 1811–1812. Also, whenever a reservoir is filled behind a dam, induced seismicity occurs. These and other observations indicate that the outer crust is always on

the brink of failure, i.e., in a state of self-organized criticality.

One implication of self-organized criticality is that all earthquakes, including the largest, represent noise on a background level of stress. The classical view of the earthquake cycle [11] is that stress gradually increases between earthquakes and drops during the earthquakes. One consequence of this view is that the level of regional seismicity should accelerate between earthquakes. In fact the temporal variation in seismicity prior to a major earthquake is a subject of considerable controversy. Some authors accept precursory quiescence as a widely applicable phenomenon [12], but others support some regional buildup in seismicity as a precursor to a major earthquake [13]. However, it is generally accepted that levels of seismicity are not predictors of future earthquakes.

Crustal deformation at shallow depths occurs through displacements on faults over a wide variety of scales. Scholz [10] refers to this seismogenic zone as the schizosphere and it typically has a thickness of 10 km. Below the schizosphere, deformation is dominated by viscous and plastic processes. Within the schizosphere, deformation is generally associated with earthquakes. Earthquakes in a zone of crustal deformation obey the Gutenberg-Richter frequency-magnitude relation to a good approximation

$$\log_{10} N = -bm + a \ , \tag{1}$$

where N is the number of earthquakes in a specified length of time in a specified region with a magnitude greater than m, and a and b are constants. Aki [14] showed that (1) is equivalent to the fractal distribution

$$N = CA^{-D/2} \ , \tag{2}$$

where A is the area of the earthquake rupture and D is the fractal dimension if we take

$$D = 2b \ . \tag{3}$$

Since the b value is usually in the range $0.65 < b < 1.05$ [15] we have $1.3 < D < 2.1$. The universality of the fractal frequency-magnitude statistics is strong evidence for self-organized critical behavior of the outer crust.

Earthquakes in the outer crust occur on a hierarchy of faults and fault segments that interlace the crust. To a first approximation, each fault or fault segment is associated with a characteristic earthquake. There is observational evidence [16] for power-law (fractal) scaling between the net offset on a fault and the fault length. As a working hypothesis we assume that each fault is associated with a characteristic earthquake. Thus a fractal distribution of earthquakes implies a fractal distribution of faults. It does not follow, however, that the fractal dimension for the frequency-size distribution of faults is the same as that for earthquakes, since this would imply that the interval of time between earthquakes is independent of scale.

Structural geologists recognize that the earth's crust is broken up into blocks on the range of scales from millimeters to hundreds of kilometers. Barton and Hsieh [17] considered the distribution of exposed joints and fractures near Yucca Mountain, Nevada, and found good agreement with a fractal distribution of block exposure taking $D = 1.6$. Sammis *et al.* [18] have proposed that a comminution model for fragmentation is applicable to tectonic deformation. This hypothesis states that direct contact between two blocks of near equal size during tectonic deformation will result in the breakup of one of the blocks. It is unlikely that small blocks will break large blocks or that large blocks will break small blocks. Their discrete model for comminution is given in Fig. 1. Two diagonally opposed blocks in a unit cube ($r = 1$) are retained at each scale so that no two blocks of equal size are in contact with each other. We have two blocks with $r = \frac{1}{2}$ and 12 blocks with $r = \frac{1}{4}$, so that $D = \ln 6/\ln 2 = 2.585$. Turcotte [19] has shown that many experimental studies of fragmentation yield fractal frequency-size distributions with $D \approx 2.5$. Considering each side of a block in Fig. 1 to be a fault, we have a fractal distribution of fault sizes with $D = \ln 3/\ln 2 = 1.585$.

Crustal seismicity is a result of the interactions between crustal blocks over a wide range of scales. In order to study these interactions we base the geometry for our cellular-automata model on comminution. Our objective is to exhibit self-organized criticality while retaining a fractal structure for the distribution of fault sizes.

II. MODEL

The standard cellular-automata model has a grid of boxes of equal size. Particles are randomly dropped into these boxes. We consider a grid of boxes with a fractal distribution of sizes [20], each box representing a fault. The random addition of particles to the boxes is analogous to the addition of stress to a zone of crustal deformation. A redistribution of particles from a box is the analog of an earthquake. The number of particles redistributed from a box is a measure of the strength of the model earthquake. Big boxes have big earthquakes, small

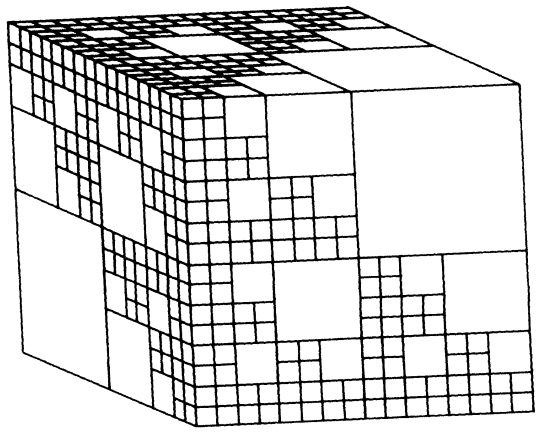

FIG. 1. Illustration of a discrete model for comminution. Diagonally opposite blocks are retained at each scale. The blocks satisfy a fractal relationship with $D = \ln 6/\ln 2 = 2.585$. The block surfaces satisfy a fractal relationship with $D = \ln 3/\ln 2 = 1.585$.

boxes have small earthquakes. Some of the redistributed particles are lost from the grid and the remainder are transferred to other boxes. This transfer is analogous to the transfer of stress during an earthquake from the fault on which the earthquake occurred to adjacent faults. When a redistribution from a small box results in an instability in a big box the instability in the small box is the analog of a foreshock. When a redistribution from a large box triggers instabilities in the smaller boxes, these are the equivalent of aftershocks.

We will consider the four models illustrated in Fig. 2. In model 1 illustrated in Fig. 2(a) a square box is divided into four equal sized boxes at first order. At second order two diagonally opposite boxes are further divided into four boxes. In Fig. 2(a) this construction has been extended to fifth order. We assume that the smallest boxes have unit size, so at fifth order we have a 32×32 grid. For this example we have $N_1=64$ for $r_1=1$, $N_2=16$ for $r_2=2$, $N_3=8$ for $r_3=4$, $N_4=4$ for $r_4=8$, and $N_5=2$ for $r_5=16$. Except for N_1, the N_i are related to the r_i by the fractal relation (2) with $D=1$. This construction can be extended to any order desired. The numerical results reported for this model were primarily carried out on an eighth-order grid (256×256). Model 2 illustrated in Fig. 2(b) is a variation of model 1 with the same fractal dimension. However, the number of largest boxes has been increased so that we have $N_1=128$ for $r_1=1$, $N_2=32$ for $r_2=2$, $N_3=16$ for $r_3=4$, and $N_4=8$ for $r_4=8$. For this fourth-order example we again have a 32×32 grid. In model 3 the square box is again divided into four equal sized boxes at first order. But at second order only one box is retained and three are further divided into four boxes. In Fig. 2(c) this model has been extended to fifth-order with a 32×32 grid. This model corresponds to the discrete model for comminution illustrated in Fig. 1. For this example we have $N_1=108$ for $r_1=1$, $N_2=27$ for $r_2=2$, $N_3=9$ for $r_3=4$, $N_4=3$ for $r_4=8$, and $N_5=1$ for $r_5=16$. Except for N_1, the N_i are related to the r_i by (2)

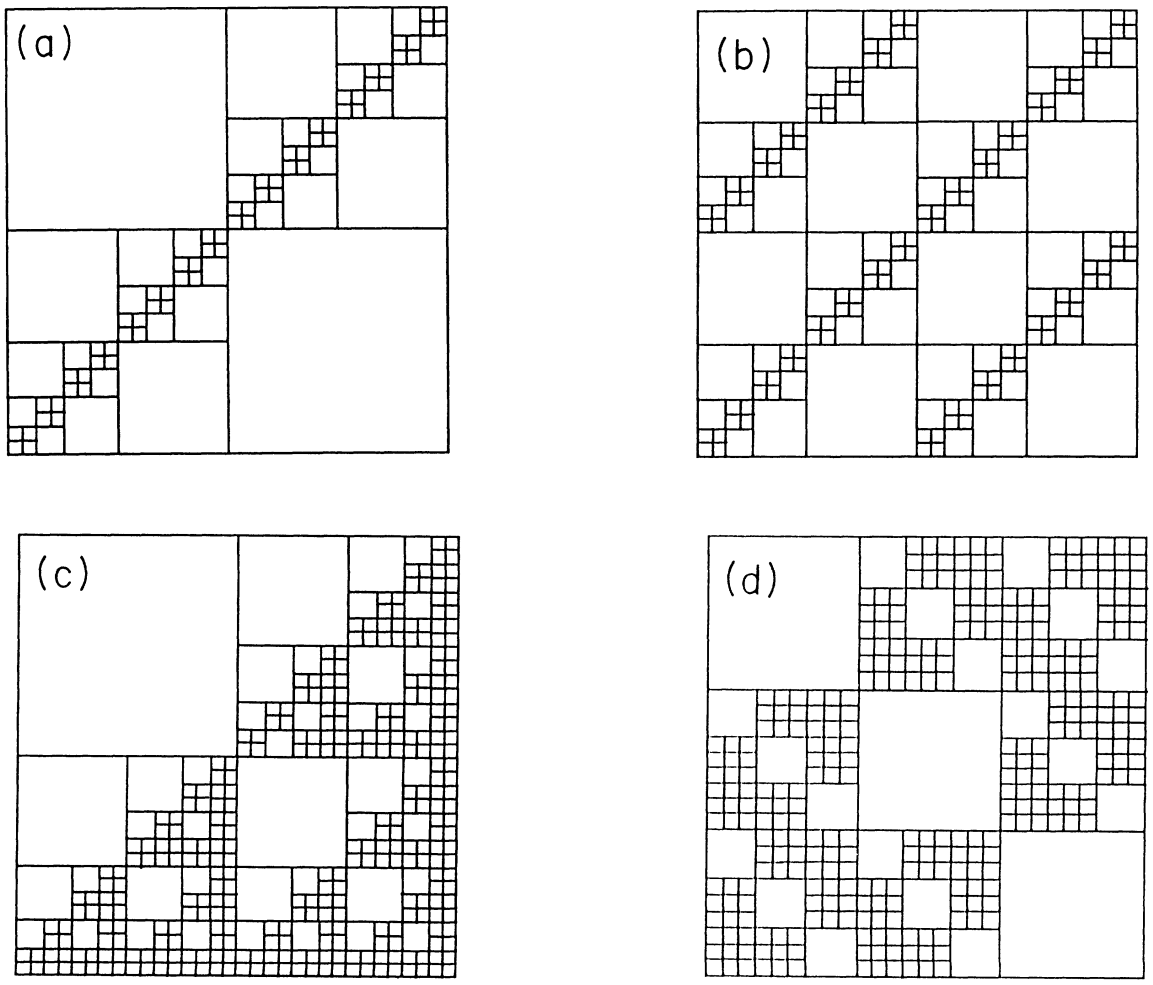

FIG. 2. Illustration of the four fractal cellular-automata models used in this paper. (a) In model 1 a square box is divided into four equal sized boxes and two diagonally opposite boxes are retained at each order. This construction has been extended to fifth order and the fractal dimension is $D=1$. (b) Model 2 is the same as model 1 (a) except that the number of the largest boxes has been increased to 8. (c) Model 3 corresponds to the discrete model for comminution illustrated in Fig. 1 carried to fifth order $D=\ln3/\ln2=1.585$. (d) In model 4 a square box is divided into nine equal sized square boxes and three boxes along a diagonal are retained at each order, $D=\ln6/\ln3=1.6309$. A third-order example is illustrated in (d).

with $D=\ln 3/\ln 2=1.5850$, in agreement with our previous discussion of Fig. 1. In model 4 illustrated in Fig. 2(d) a square box is divided into nine equal sized boxes at first order. At second order, three boxes along a diagonal are retained and the other six boxes are further divided into nine boxes. In Fig. 2(d) this construction has been extended to third order on a 27×27 grid. For this example we have $N_1=324$ for $r_1=1$, $N_2=18$ for $r_2=3$, and $N_3=3$ for $r_3=9$. Except for N_1, the N_i are related to the r_i by (2) with $D=\ln 6/\ln 3=1.6309$.

We apply the standard cellular-automata rules to our four models:

(i) Particles are added one at a time to randomly selected boxes. The probability that a particle is added to a box is proportional to the area A of the box. For a third-order version of model 1 these probabilities are illustrated in Fig. 3(a). The largest boxes have $r_3=4$ and $P_{r_3}=\frac{1}{4}$, for $r_2=2$ we have $P_{r_2}=\frac{1}{16}$, and for $r_1=1$, we have $P_{r_1}=\frac{1}{64}$.

(ii) A box becomes unstable when it contains $4A$ particles. For model 1 the number of particles required for instability in a third-order example is given in Fig. 3(b). For the largest boxes with $r_3=4$ we require $n_3=64$, with $r_2=2$ we require $n_2=8$, and with $r_1=1$ we require $n_1=4$.

(iii) We consider two alternative rules for redistributions. In rule (iii), particles are redistributed to immediately adjacent boxes or are lost from the grid. The number of particles redistributed to an adjacent box is proportional to the linear dimension of the box. As an example we illustrate in Fig. 3(c) the redistribution of particles from one of the largest boxes $r_3=4$. Of the 64 particles that are redistributed 32 are lost from the grid, 16

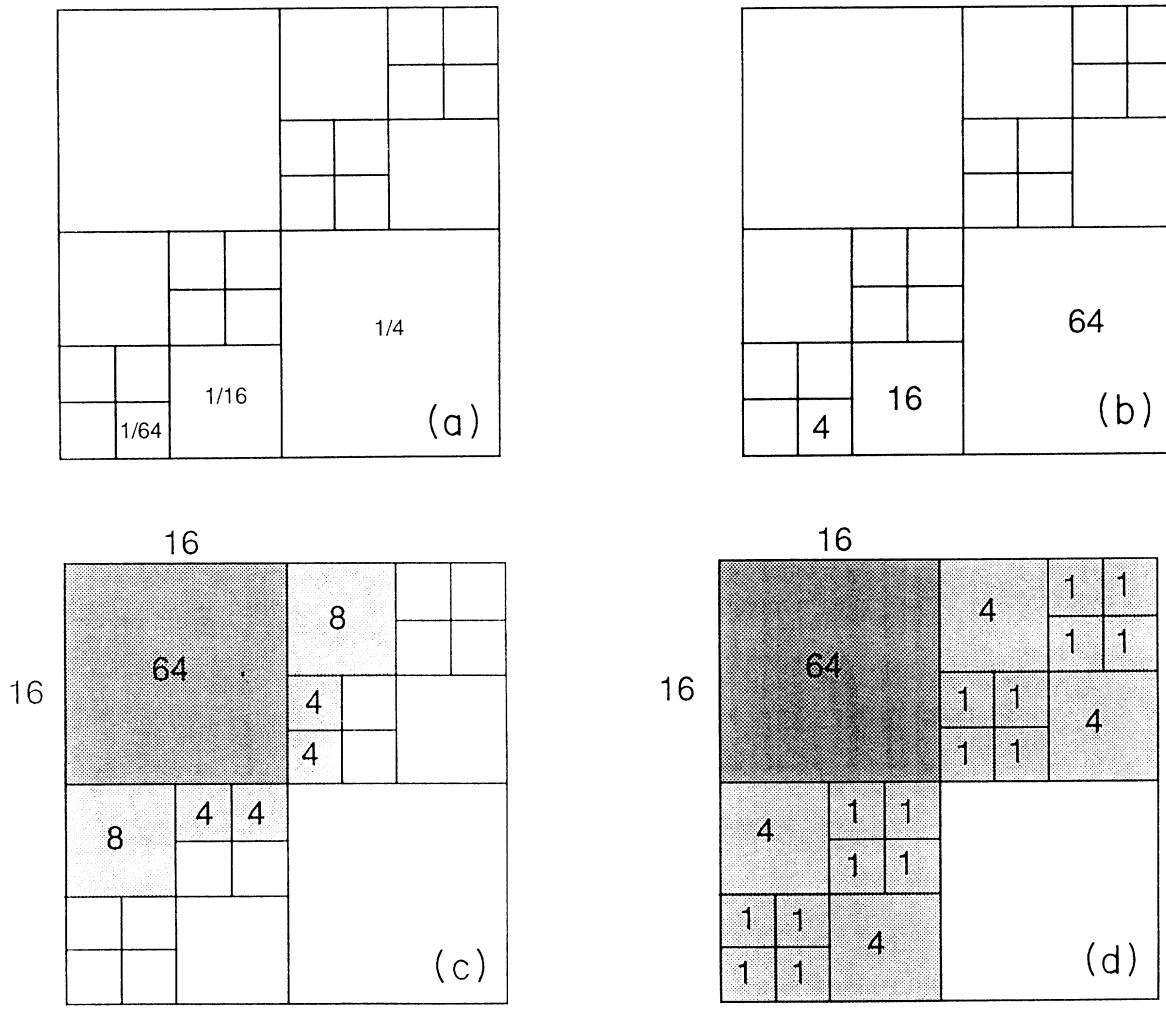

FIG. 3. Illustration of the cellular automata rules using a third-order version of model 1. (a) Rule (i): Probability that a particle is added to a box is proportional to its area A. (b) Rule (ii): A box becomes unstable when it contains $4A$ particles. (c) Rule (iii): The numbers of particles redistributed from a large (heavily shaded) box to the immediately adjacent boxes (lightly shaded) are proportional to the linear dimensions of the boxes. (d) Rule (iii'): Particles are redistributed from a large (darkly shaded box) to the four adjacent (lightly shaded) regions that have the same area as the unstable box; the redistribution is proportional to the area of the box. Two of the adjacent areas are off the grid so these particles are lost.

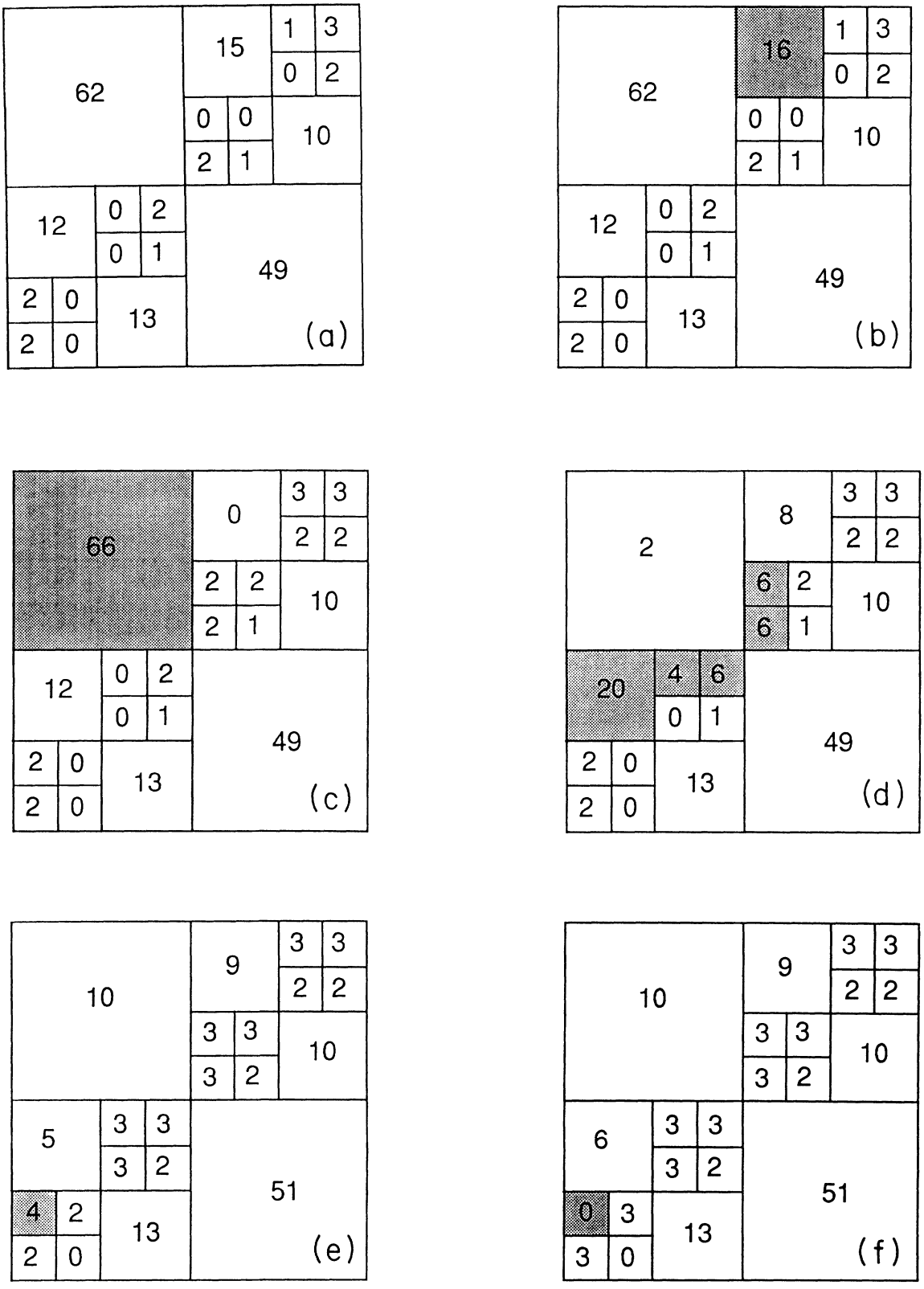

FIG. 4. Illustration of the model evolution using a third-order version of model 1. (a) A particle distribution with all boxes stable. (b) A particle has been randomly added to the shaded box making it unstable. (c) Particles have been redistributed resulting in the instability of the shaded large box. (d) Sixty-four particles have been redistributed from the large box resulting in the instability of the five shaded boxes. (e) Particles have been redistributed from the five unstable boxes in (d), resulting in the single shaded box being unstable. (f) The final redistribution is carried out resulting in all boxes being stable.

are redistributed into two boxes with $r_2=2$, and 16 are redistributed into four boxes with $r_1=1$.

(iii') In rule (iii') particles are redistributed into the four adjacent regions that have the same size as the unstable box. The number of particles redistributed to a box is proportional to the area of the box. As an example we illustrate in Fig. 3(d) the redistribution of 64 particles from one of the largest boxes $r_3=4$. Of the 64 particles that are redistributed 32 are lost from the grid, 16 are redistributed into four boxes with $r_2=2$, and 16 are redistributed into the 16 boxes with $r_1=1$.

(iv) If after a redistribution of particles from a box any of the adjacent boxes are unstable, one or more further redistributions are carried out. In any redistribution the critical number of particles is redistributed. Redistributions are continued until all boxes are stable.

In order to illustrate these rules we consider the example given in Fig. 4. We begin with the stable state on the third-order (8×8) grid illustrated in Fig. 4(a). All boxes have less than their critical value of particles so that it is appropriate to randomly add a particle [rule (i)]. The box with 15 particle receives the additional particle, and Fig. 4(b) is now unstable [rule (ii)]. We redistribute the particles in this box according to rule (iii), the resultant distribution illustrated in Fig. 4(c); four particles have been lost from the grid and the large upper box is unstable with 66 particles [rule (iii)]. The redistribution from a small box to a large box resulting in the instability of the large box is the analog of a foreshock. We next redistribute 64 particles from the large box leaving two particles in it [rule (iv)]. Thirty-two particles are lost from the grid and the resulting distribution is illustrated in Fig. 4(d). Because a large number of particles have been redistributed nearly all ($\frac{5}{6}$) of the neighboring boxes are unstable. A redistribution from a large box (a main shock) always trigger a sequence of further instabilities (aftershocks). Further redistributions from the five unstable boxes are carried out leaving one unstable box, Fig. 4(e). After the redistribution is carried out from this small box the system is stable [Fig. 4(f)] and it is appropriate to randomly add another particle. During the sequence of events illustrated in Fig. 4 there were five events of size 1, two events of size 4, and one event of size 16; a total of 41 particles were lost from the grid.

III. SYNTHETIC EARTHQUAKE CATALOGS

We have carried out a series of calculations using our four models in order to better understand the statistics of behavior and to relate these statistics to the statistics of distributed seismicity. Our results were obtained with fourth-order, sixth-order, and eighth-order models. The statistical results obtained from fourth-order models were virtually indistinguishable from the results obtained with sixth- and eighth-order models.

A. Sum of particles

We first report variations in the total number of particles on the grid for a fourth-order version of model 1 [Fig. 1(a)]. The width of the grid is $2^4=16$ with the scale

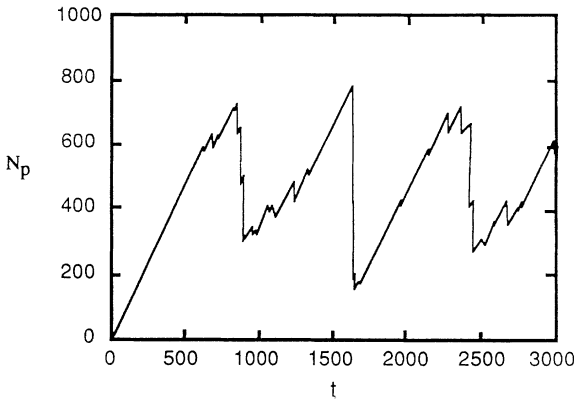

FIG. 5. Dependence of the total number of particles N_p in a fourth-order version of model 1 on time. Each time step represents the addition of one particle.

normalized to the smallest box. The maximum possible number of particles on the grid without an instability is $N_{p\max}=255\times2+63\times4+15\times8+3\times32=978$. We start with empty boxes and randomly add particles one at a time according to rule (i). An example of the evolution of the system is given in Fig. 5, where the total number of particles N_p is given as a function of time, each time step representing the addition on one particle. It is seen that about 600 particles have been added before instabilities set in. The total number of particles N_p is equivalent to a state variable and is analogous to the regional stress in the seismogenic crust. The sequence of events illustrated in Fig. 5 is analogous to the release of regional strain accumulation by earthquakes.

B. Frequency-magnitude statistics

The behavior of a cellular-automata model is usually characterized by the frequency-magnitude statistics of redistribution events. We first consider an eighth-order (256×256) version of model 1. Our results were obtained in a run in which 1.3×10^7 particles were added to the grid. This resulted in 300 eighth-order ($r=128$) redistributions (great earthquakes) and about 250 000 other distributions (smaller earthquakes).

The cumulative frequency-magnitude statistics for main shocks are given in Fig. 6(a). Only main shocks are included because this is standard seismology practice. It should be noted, however, that the inclusion of foreshocks and aftershocks would have a negligible influence on the statistics. The number of events N_c in boxes equal to or greater than r divided by the total number of events N_r is given as a function of the box sizes. Note that the number of events of size $r=1$ has been reduced by a factor of 2 because the number of boxes of this size is twice the scaled fractal value. An excellent correlation with the fractal relation (2) is obtained taking $D=1.67$. From (3) this corresponds to $b=0.835$, which is quite a reasonable value for distributed seismicity. Evernden [15] has obtained b values for regional seismicity and concludes that $b=0.85\pm0.20$.

We found that 28% of the largest events ($r=128$) re-

TABLE I. Frequency-magnitude statistics for our models.

			Main shocks		Foreshocks		Aftershocks		Foreshocks
Model	D_m	Order	D	b	D	b	D	b	(%)
1	1	8	1.67	0.835	0.82	0.41	1.27	0.635	28
1′	1	4	1.67	0.835	1.15	0.575	1.48	0.74	28
2	1	7	1.67	0.835	0.87	0.435	1.40	0.70	29
3	1.585	6	2.50	1.25	0.94	0.47	2.02	1.01	31.5
4	1.630	4	4.05	2.025	2.74	1.37	1.15	0.575	23.1

sulted from one or more redistributions from smaller events. In terms of our analogy to distributed seismicity this means that 28% of the main shocks had foreshocks. This is in reasonable agreement with studies of actual earthquakes done by von Seggern, Alexander, and Baag [21], who found that 21% of the earthquakes studied had foreshocks, and by Jones and Molnar [22] who found that 44% of larger shallow earthquakes that could be recorded teleseismically had foreshocks. The frequency-size distribution of foreshocks is in reasonable agreement with the fractal relation (2) taking $D=0.82$ ($b=0.41$). Our result of a small b value is physically reasonable since large earthquakes are more likely to act as foreshocks than smaller earthquakes.

All large ($r=128$) main shocks had extensive sequences of aftershocks, an average 300 aftershocks occurring for each main shock. The frequency-size distribution of aftershocks is also in good agreement with the fractal relation (2), taking $D=1.27$ ($b=0.635$). Reasenberg and Jones [23] have studied 63 aftershock sequences in California and found good correlations with the Gutenberg-Richter relation (1) with $b=0.90\pm0.2$. Thus the lower value we find is not consistent with observations.

The cumulative frequency-magnitude statistics for main shocks ($r=32$) of a sixth-order (128×128) version of model 2 are given in Fig. 6(b). We find an excellent correlation with the fractal relation (2), taking $D=1.67$

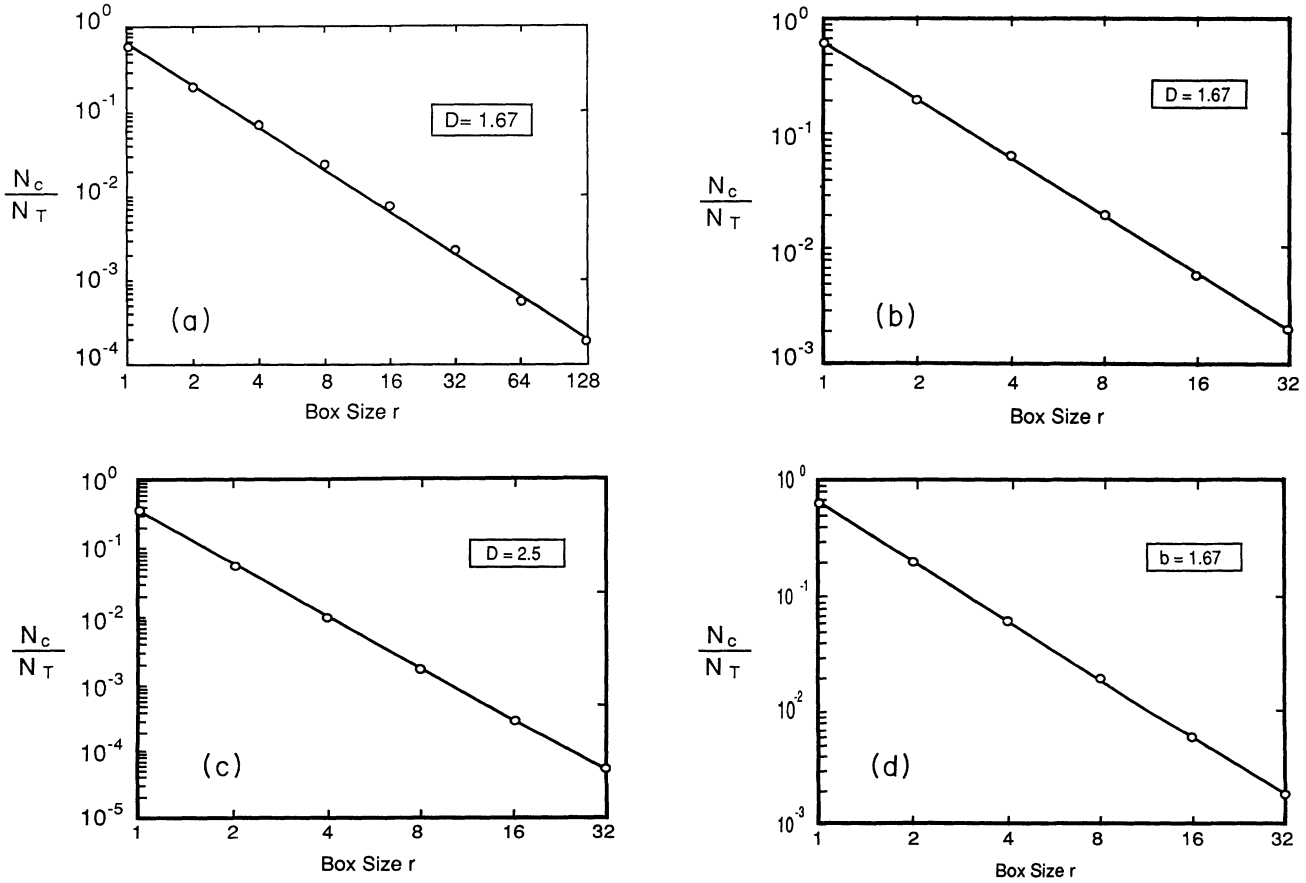

FIG. 6. Frequency-magnitude statistics for events using model 1 (a), model 2 (b), model 3 (c), and model 1′ (d). In each case the results are correlated with (2).

($b=0.835$). This is the same value obtained for model 1 in Fig. 6(a). We found that 29% of the largest events had foreshocks. The aftershocks correlate well with (2) taking $D=1.4$ ($b=0.7$). This is somewhat higher than model 1 and is in better agreement with observations.

The cumulative frequency-magnitude statistics for main shocks of a seventh-order (128×128) version of model 3 are given in Fig. 6(c). We find an excellent correlation with the fractal relation (2), taking $D=2.50$ ($b=1.25$). This is considerably higher than the values found in models 1 and 2 and is also significantly higher than observed values for distributed seismicity. We found that 31.5% of the largest events had foreshocks. The aftershocks correlate well with (2), taking $D=2.02$ ($b=1.01$).

The results for the fourth-order (243×243) version of model 4 are summarized in Table I, along with the results for the other models. The fractal dimensions (and equivalent b values) for model 4 are quite large compared both with the other models and with observed seismicity.

We now reconsider model 1 using the redistribution of particles illustrated in Fig. 3(d) [rule (iii')] instead of the redistribution illustrated in Fig. 3(c) [rule (iii)]. We designate this as model 1' and consider a fourth-order (32×32) version. The cumulative frequency-magnitude statistics for main shocks are given in Fig. 6(d). An excellent correlation is obtained with (2), taking $D=1.67$ ($b=0.835$), the same values obtained for model 1. We find that the aftershocks correlate well with (2), taking $0=1.48$ ($b=0.72$). This is somewhat higher than model 1 and is in better agreement with observations. However, the results do not appear to be very sensitive to the details of particle redistributions.

C. Decay of aftershocks

We next consider the temporal decays of aftershocks after a main shock. We again consider the 300 largest earthquakes ($r=128$) obtained for our eighth-order version of model 1. In Fig. 7 the number of aftershocks N_{AF} at each redistribution is given. Twenty redistributions are considered and aftershocks of all magnitudes

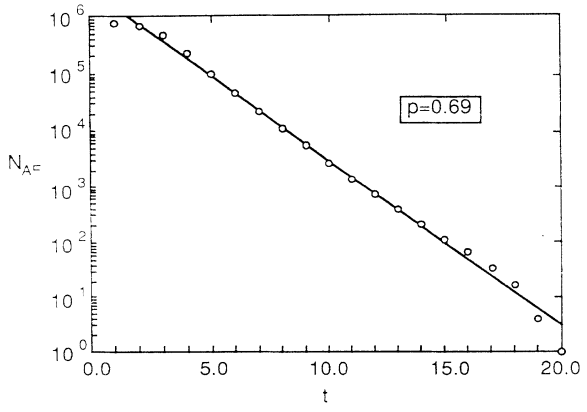

FIG. 7. The number of aftershocks N_{AF} at each redistribution t as a function of t. Only the largest main shocks ($r=128$) are considered.

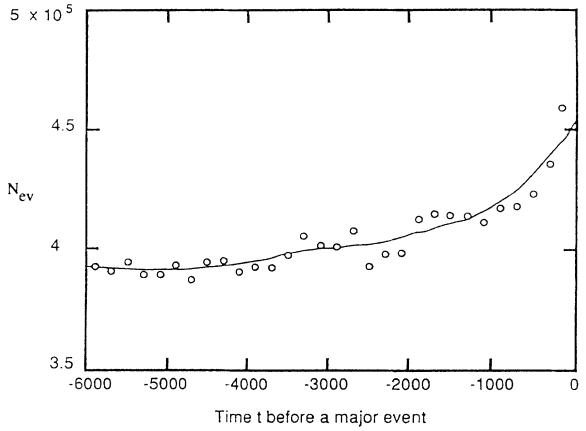

FIG. 8. The number of events in time windows $\Delta t=200$ prior to a major event. The solid line is a fit to the data indicating about a 15% increase in activity prior to a major event.

($r=1-64$) are considered. After the first two redistributions the number of aftershocks at each redistribution is in good agreement with the exponential decay relation

$$N_{AF}=Ce^{-pt}, \tag{4}$$

taking $C=3\times10^6$ and $p=0.69$. The number of aftershocks decreases by a factor of 2 at each distribution.

Actual earthquake aftershocks, however, decay in time according to the modified Omori law [24]

$$N_{AF}=\frac{k}{(c-t)^p}, \tag{5}$$

where k, c, and p are constants and usually $p=1.0\pm0.1$. Clearly the model behavior differs from the observed decay of aftershocks. The physics of the model is that the redistribution of particles (stress) causes a sequence of instabilities (aftershocks); the subsequent redistributions cause more instabilities (aftershocks). Thus it is not surprising that at each redistribution the number of aftershocks decreases by a constant factor ($\frac{1}{2}$).

Actual aftershocks involve a time delay between the application of the stress (the main shock or an aftershock) and the subsequent frictional rupture. This delay is likely to be related to the size of the incipient rupture. The incubation time is not accounted for in our model.

D. Frequency of events

It is also of interest to determine whether there is an increase or decrease in the number of smaller events immediately prior to a large event. For this study we consider the sixth-order (64×64) version of model 1. The numbers of events in time windows prior to a large event are given in Fig. 8 as a function of the time before the large event. It is seen that there is a small ($\sim10\%$) increase in the number of smaller events immediately prior to a large event. For this model the mean interval between large events is near 10^4 time steps, the increase in the frequency of smaller events occurring in about the last 10% of this interval.

IV. IMPLICATIONS FOR EARTHQUAKE PREDICTION

At the present time there is no recognized basis for earthquake prediction. A remarkable feature of earthquakes is the apparent absence of any systematic precursors [25]. Extensive and systematic searches have been carried out for precursory tilts and variations in rates of strain accumulation, variations in electrical currents and magnetic fields in the vicinity of faults, changes in the level of the water table and flow rates of springs, emissions of radon gas, animal behavior, variations in seismic velocities, and precursory variations in seismic activity. No systematic precursory activity has been recognized.

With extensive seismic networks in seismically active areas, a very large data base for precursory seismic activity exists but searches have not been successful. Analog models such as those presented in this paper provide a test bed for studying the statistics of precursory events. As discussed in Sec. III, our model does not appear to generate predictive precursory-event statistics. A possible conclusion is that events in a system in a state of self-organized criticality are inherently not predictable. It should be noted that observations of the number of particles in a compartment would indicate which compartments in our model are on the brink of failure. But even this approach would not account for precursory events that transferred particles to a larger compartment.

V. CONCLUSIONS

Distributed seismicity appears to fit the general definition of self-organized critical phenomena. Elastic energy is continuously added by the relative movement of the surface plates in the upper crust. A large fraction of the energy is dissipated in discrete events—earthquakes. The frequency-magnitude statistics of earthquakes are fractal. The critical state is the maximum elastic energy that can be stored in the region. Seismicity results in a fluctuating value of the stored energy below the critical state.

One approach to the modeling of self-organized critical phenomena is to use cellular-automata models. In this paper we have considered a cellular-automata model that reproduces several aspects of distributed seismicity. Instead of assuming a grid of boxes of equal size, we hypothesize a fractal distribution of box sizes. A redistribution from a box of a prescribed size is taken to be a model earthquake of a prescribed magnitude. Subsequent redistributions are taken to be aftershocks. If a redistribution from a small box triggers a redistribution from a large box we have had a foreshock. This simple model simulates many of the observed statistics of distributed seismicity.

One of the remarkable aspects of large earthquakes is the apparent absence of any systematic precursors [25]. An important question is whether the absence of precursors is an intrinsic property of systems that exhibit self-organized criticality. For the cellular-automata model studied in this paper we do not observe systematic precursors before the largest events. The frequency of smaller events increases about 10% but the statistical fluctuations are sufficiently large that the increase cannot be considered a systematic precursor.

ACKNOWLEDGMENTS

This research was supported by the U.S. Geological Survey (USGS), Department of the Interior under USGS Grant No. 1434-92-G-2165.

[1] P. Bak, C. Tang, and K. Wiesenfeld, Phys. Rev. A **38**, 364 (1989).

[2] L. P. Kadanoff, S. R. Nagel, L. Wu, and S. M. Zhou, Phys. Rev. A **39**, 6524 (1989).

[3] P. Evesque, Phys. Rev. A **43**, 2720 (1991); S. R. Nagel, Rev. Mod. Phys. **64**, 321 (1992); J. Rosendahl, M. Vekie, and J. Kelley, Phys. Rev. E **47**, 1401 (1993).

[4] P. Bak and C. Tang, J. Geophys. Res. **94**, 15 635 (1989).

[5] R. Burridge and L. Knopoff, Seis. Soc. Am. Bull. **57**, 341 (1967).

[6] J. Huang and D. L. Turcotte, Geophys. Res. Lett. **17**, 223 (1990); Nature **348**, 234 (1990); Pure Appl. Geophys. **138**, 569 (1992); G. Narkounskaia and D. L. Turcotte, Geophys. J. Int. **111**, 250 (1992).

[7] J. M. Carlson and J. S. Langer, Phys. Rev. A **40**, 6470 (1989).

[8] H. Nakanishi, Phys. Rev. A **41**, 7086 (1990); **43**, 6613 (1991).

[9] H. Takayasu and M. Matsuzaki, Phys. Lett. A **131**, 224 (1988); K. Ito and M. Matsuzaki, J. Geophys. Res. **95**, 6853 (1990); S. R. Brown, C. H. Scholz, and J. B. Rundle, Geophys. Res. Lett. **18**, 215 (1991); J. M. Carlson, J. Geophys. Res. **96**, 4255 (1991); Phys. Rev. A **44**, 6266 (1991); J. M. Carlson, J. S. Langer, B. E. Shaw, and C. Tang, *ibid.* **44**, 884 (1991); J. S. Langer and C. Tang, Phys. Rev. Lett. **67**, 1043 (1991); M. Matsuzaki and H. Takayasu, J. Geophys. Res. **96**, 19 925 (1991); J. B. Rundle and S. R. Brown, J. Stat. Phys. **65**, 403 (1991); J. Huang, G. Narkounskaia, and D. L. Turcotte, Geophys. J. Int. **111**, 259 (1992); G. Narkounskaia, J. Huang, and D. L. Turcotte, J. Stat. Phys. **67**, 1151 (1992); J. M. Carlson, E. R. Grannan, and G. H. Swindle, Phys. Rev. E **47**, 93 (1993).

[10] C. H. Scholz, in *Spontaneous Formation of Space-Time Structures and Criticality,* edited by T. Riste and D. Sherrington (Kluwer, Dordrecht, 1991), p. 41.

[11] D. L. Turcotte, J. Y. Liu, and F. H. Kulhawy, J. Geophys. Res. **89**, 5801 (1984); J. R. Rice, *ibid.* **98**, 9885 (1993).

[12] C. H. Scholz, Pure Appl. Geophys. **126**, 701 (1988); M. Wyss and R. E. Haberman, *ibid.* **126**, 319 (1988); S. Y. Schreider, Phys. Earth Planet, Inter. **61**, 113 (1990).

[13] V. I. Keilis-Borok, Rev. Geophys. **28**, 19 (1990); L. R. Sykes and S. C. Jaume, Nature **348**, 595 (1990).

[14] K. Aki, in *Earthquake Prediction,* edited by D. W. Simpson and P. G. Richards (American Geophysical Union, Washington, DC, 1981), p. 566.

[15] J. F. Evernden, Seis. Soc. Am. Bull. **60**, 393 (1970).

[16] J. J. Walsh and J. Watterson, J. Struct. Geol. **10**, 329 (1988).
[17] C. C. Barton and P. A. Hsieh, *28th International Geological Congress Field Trip Guidebook* (American Geophysical Union, Washington, DC, 1989), Vol. T385.
[18] C. G. Sammis, R. H. Osborne, J. L. Anderson, M. Banerdt, and P. White, Pure Appl. Geophys. **124**, 53 (1986).
[19] D. L. Turcotte, J. Geophys. Res. **91**, 1921 (1986).
[20] B. Barriere and D. L. Turcotte, Geophys. Res. Lett. **18**, 2011 (1991).
[21] F. von Seggern, S. S. Alexander, and C. E. Baag, J. Geophys. Res. **86**, 9325 (1981).
[22] L. Jones and P. Molnar, Nature **262**, 677 (1976).
[23] P. A. Reasenberg and L. M. Jones, Science **243**, 1173 (1989).
[24] T. Utsu, J. Fac. Sci. Hokkaido Univ. Ser. 7 **3**, 197 (1970).
[25] D. L. Turcotte, Annu. Rev. Earth Planet. Sci. **19**, 263 (1991).

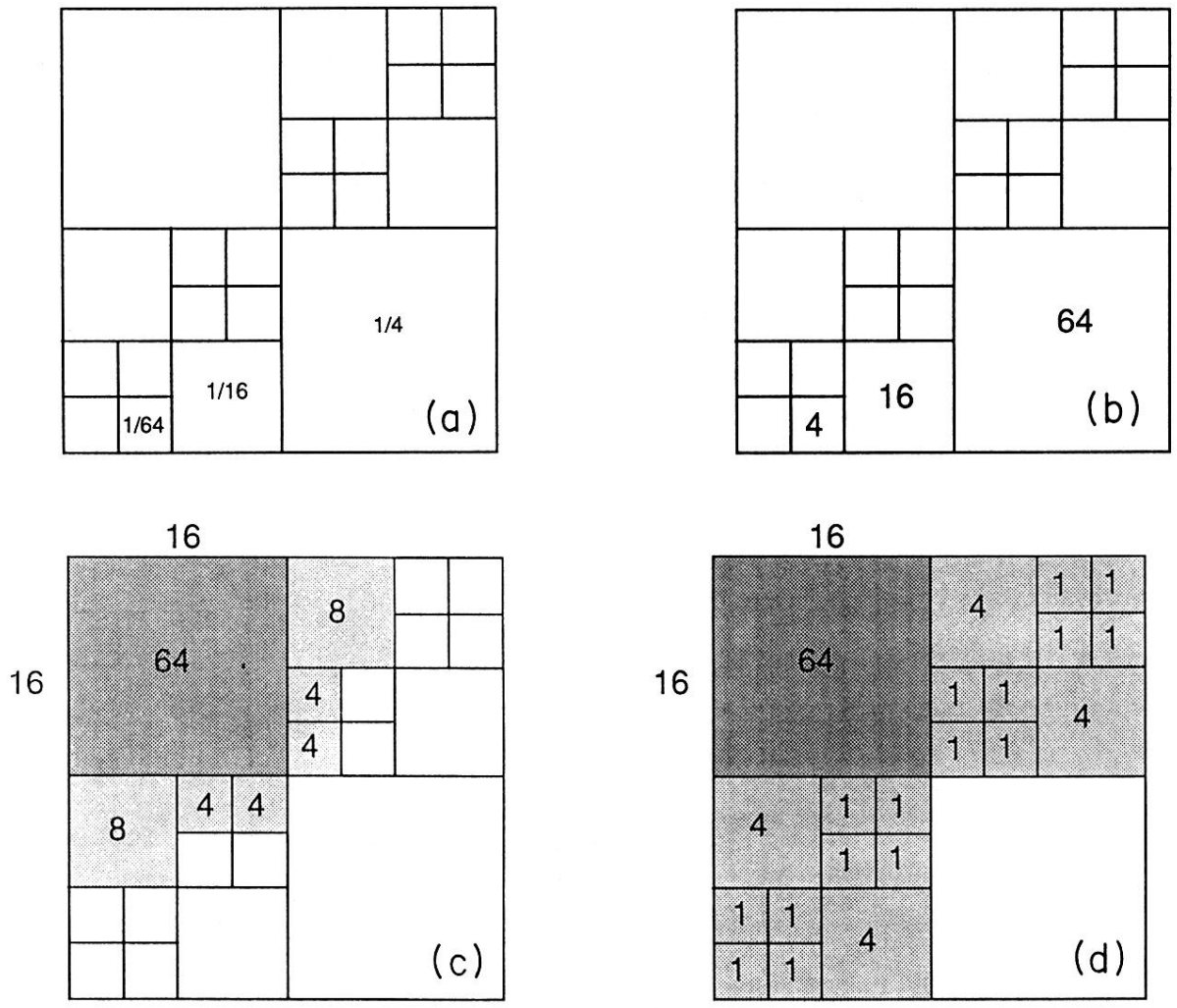

FIG. 3. Illustration of the cellular automata rules using a third-order version of model 1. (a) Rule (i): Probability that a particle is added to a box is proportional to its area A. (b) Rule (ii): A box becomes unstable when it contains $4A$ particles. (c) Rule (iii): The numbers of particles redistributed from a large (heavily shaded) box to the immediately adjacent boxes (lightly shaded) are proportional to the linear dimensions of the boxes. (d) Rule (iii'): Particles are redistributed from a large (darkly shaded box) to the four adjacent (lightly shaded) regions that have the same area as the unstable box; the redistribution is proportional to the area of the box. Two of the adjacent areas are off the grid so these particles are lost.

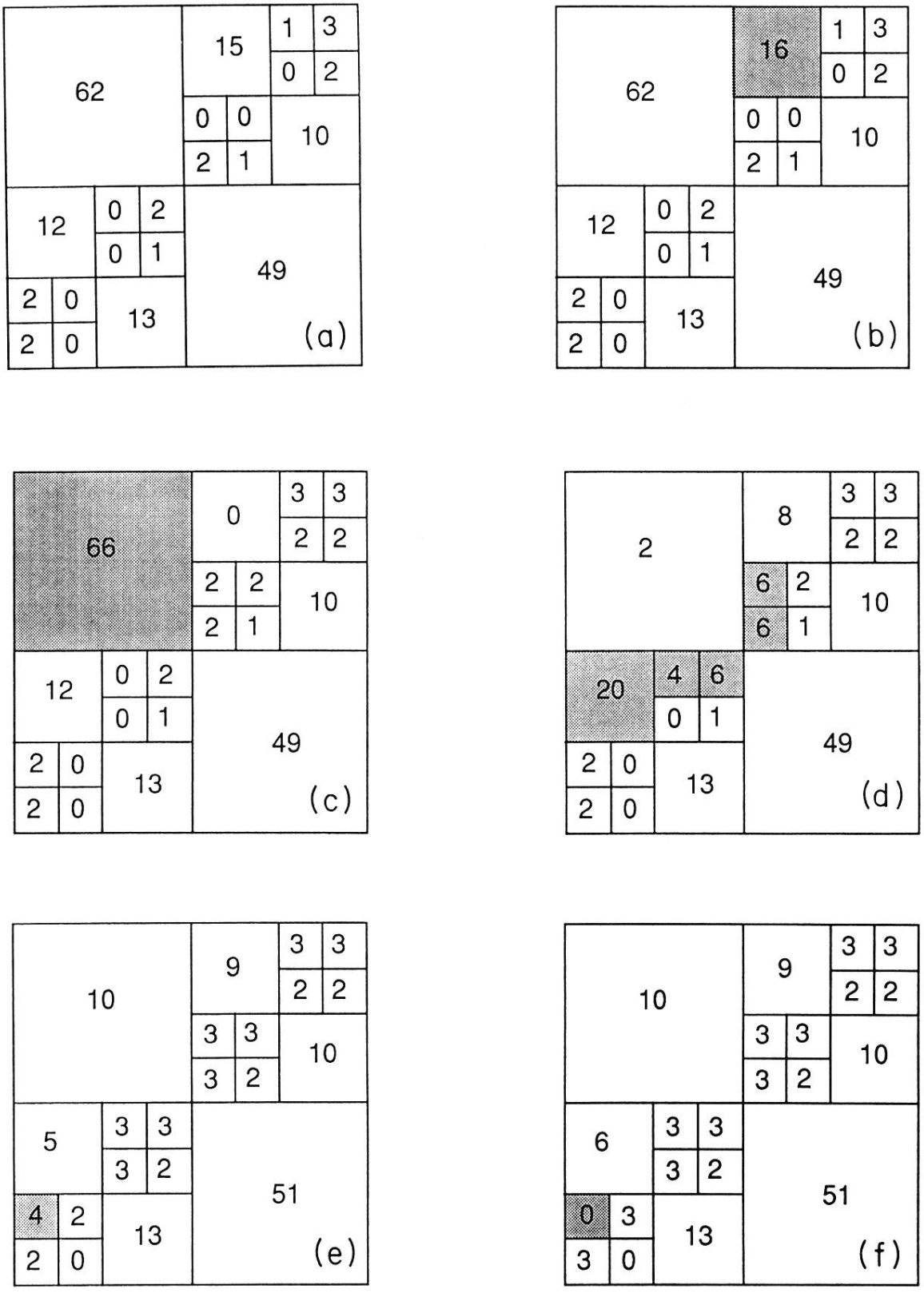

FIG. 4. Illustration of the model evolution using a third-order version of model 1. (a) A particle distribution with all boxes stable. (b) A particle has been randomly added to the shaded box making it unstable. (c) Particles have been redistributed resulting in the instability of the shaded large box. (d) Sixty-four particles have been redistributed from the large box resulting in the instability of the five shaded boxes. (e) Particles have been redistributed from the five unstable boxes in (d), resulting in the single shaded box being unstable. (f) The final redistribution is carried out resulting in all boxes being stable.